Spin-orbit coupling in transition metal dichalcogenide heterobilayer flat bands

Rademaker, Louk

How to cite

RADEMAKER, Louk. Spin-orbit coupling in transition metal dichalcogenide heterobilayer flat bands. In: Physical review. B, 2022, vol. 105, n° 19, p. 195428. doi: 10.1103/PhysRevB.105.195428

This publication URL: https://archive-ouverte.unige.ch/unige:165766
Publication DOI: 10.1103/PhysRevB.105.195428

Spin-orbit coupling in transition metal dichalcogenide heterobilayer flat bands

Louk Rademaker
Department of Theoretical Physics, University of Geneva, CH-1211 Geneva, Switzerland

(Received 17 November 2021; revised 4 May 2022; accepted 9 May 2022; published 23 May 2022)

The valence flat bands in transition metal dichalcogenide (TMD) heterobilayers are shown to exhibit strong intralayer spin-orbit coupling. I show that symmetry constrains the spin-dependent complex phase of hopping terms in an effective tight-binding model of the valence flat bands. A perpendicular electric field causes interlayer hybridization, such that the effective model becomes equivalent to the Kane-Mele model of topological insulators. The proposed model can be used as a starting point to understand interactions and the experimentally observed topological transitions.

DOI: 10.1103/PhysRevB.105.195428

I. INTRODUCTION

Heterostructures with moiré patterns, emerging from the lattice mismatch or misalignment of two-dimensional materials, have proven to be a fertile ground for novel electronic states [1–3]. Among possible materials, "flat bands" are expected to occur in bilayers of transition metal dichalcogenide (TMD) monolayer semiconductors. TMD heterobilayers, when the two layers are of a different material, have been proposed as an ideal realization of the triangular lattice Hubbard model with real short-range hoppings [4].

Indeed, experimental results in WS_2/WSe_2 and $MoTe_2/WSe_2$ bilayers include the observation of a Mott insulating state at half filling of the flat bands [5,6] and generalized Wigner crystals at other fillings [7–10]. Recently, it came as quite a surprise that upon tuning a perpendicular electric field, both the quantum spin Hall effect (QSH) and quantum anomalous Hall (QAH) effect were observed in bilayer $MoTe_2/WSe_2$ [11]. After all, the original heterobilayer model [4] did not include any spin-orbit coupling, in contrast to the homobilayer model that predicted topological band structures [12].

There is a growing literature aiming to understand and characterize TMD heterobilayers [13–27], where the observed topological transitions are proposed to originate in lattice relaxation [28], or interlayer coupling leading to a canted ferromagnet [29,30], with possible interaction-induced band renormalization [31]. However, as of yet there is no derivation of a simple tight-binding model that can account for the observed topological behavior. The derivation of such a tight-binding model using symmetry arguments is the core of this paper.

Starting from the model of Ref. [4], I show that one must carefully select the correct backfolding of the monolayer momenta to the moiré mini-Brillouin zone. Doing so, this directly yields strong *spin-orbit coupling* in the form of a complex spin-dependent hopping, constrained by the symmetry of the model. The corresponding tight-binding model is equivalent to the next-nearest-neighbor hopping in the Kane-Mele (KM) model. By tuning the band offset through a perpendicular electric field, the second layer comes into play and we find a full realization of the KM model with a corresponding topological transition and band inversion to a topological insulator phase. The tight-binding model derived in this paper serves as a starting point for studying the interplay between topology and interaction effects in TMD heterobilayers.

II. CONTINUUM MODEL

Let me first recap the essence of the continuum model of flat bands in TMD heterobilayers [4]. Monolayer transition metal dichalcogenides (MX_2 with $M = $ W, Mo and $X = $ S, Se, Te) have a hexagonal lattice with C_3 rotational symmetry. They are semiconductors with a relatively large direct band gap at the $\mathbf{K}$ and $\mathbf{K}'$ points. The valence band states have a large Ising spin splitting, such that states at $\mathbf{K}$ are spin-$\uparrow$ and the states at $\mathbf{K}'$ are spin-$\downarrow$. Spins ($\uparrow$ or $\downarrow$) and valleys ($\mathbf{K}$ or $\mathbf{K}'$) are therefore inextricably coupled.

Whenever two different TMD monolayers are combined in a heterobilayer with twist angle θ, a moiré pattern is created with length scale $a_M = 1/\sqrt{\frac{1}{a_1^2} + \frac{1}{a_2^2} - \frac{2\cos\theta}{a_1 a_2}}$, where $a_{1,2}$ are the lattice constants of the monolayers. A proof of this relation is presented in the Appendix. Because different TMD monolayers have different band gaps, the top of the valence band of one layer lies in the gap of the other (a type-I or type-II band alignment). Consequently, the valence band in a heterobilayer exclusively consists of states localized in a *single* layer.

These heterobilayer valence band states can be described, per spin/valley, by imposing a moiré potential $V(\mathbf{r})$ on the monolayer valence band states,

$$H = -\frac{\hbar^2 \mathbf{Q}^2}{2m^*} + V(\mathbf{r}),$$
$$V(\mathbf{r}) = \sum_{\mathbf{g}_j} V_j \exp\left[i\mathbf{g}_j \mathbf{r}\right], \tag{1}$$

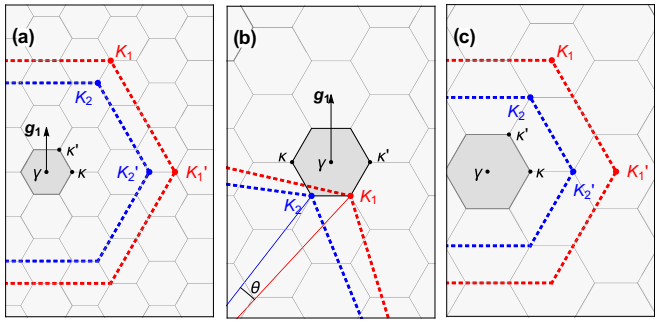

FIG. 1. (a) When two layers with inequivalent lattice constants are combined, in general the **K** points of the monolayers map onto the $\boldsymbol{\kappa}$ points of the mini-Brillouin zone. This is specifically the case for aligned WS_2/WSe_2 and $MoTe_2/WSe_2$. (b) In the case of an incommensurate moiré pattern, for example due to a twist angle θ, the natural mapping is similar. (c) Only when the moiré length satisfies $a_M = pa_1$ with $p \mod 3 = 0$, do the **K** points of layer 1 map onto the center of the mini-BZ $\boldsymbol{\gamma}$, as was done in Ref. [4].

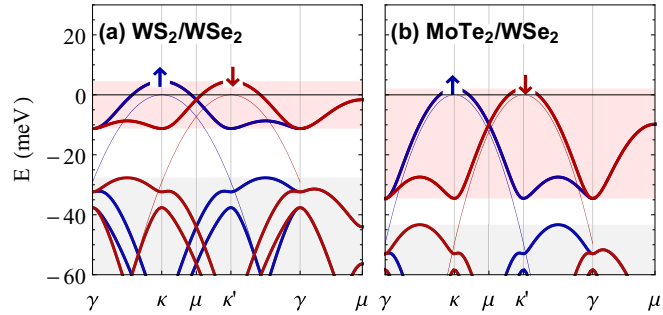

FIG. 2. (a) Flat valence band structure of aligned AA-stacked WS_2/WSe_2. The colors red/blue indicate the spin $\downarrow/\uparrow$ of the bands, showing significant spin-orbit coupling. The thin lines indicate the monolayer valence band states in the absence of the moiré potential. Upon Wannierization, the nearest-neighbor hopping equals $|t_1| = 1.8$ meV. (b) Flat valence band structure of aligned AB-stacked $MoTe_2/WSe_2$, with a similar spin-orbit splitting. The nearest-neighbor hopping equals $|t_1| = 4.0$ meV.

where $\mathbf{g}_j = \frac{4\pi}{\sqrt{3}}(-\sin\frac{2\pi(j-1)}{6}, \cos\frac{2\pi(j-1)}{6})$ are the six reciprocal moiré vectors and **Q** is the momentum relative to the $\mathbf{K}/\mathbf{K}'$ point of the monolayer. Because $V(\mathbf{r})$ must be real and C_3 symmetric, we find $V_1 = V_3 = V_5$ and $V_2 = V_4 = V_6 = V_1^*$ [4,32,33], which means one can parametrize the moiré potential using only two parameters (V, ψ) such that $V_1 = Ve^{i\psi}$. For $MoSe_2/WSe_2$ bilayers, Ref. [4] calculated $(V, \psi) = (6.6\text{ meV}, -94^\circ)$. This results in a topmost valence *flat band* with almost perfect Gaussian Wannier orbitals centered on a moiré triangular lattice.

III. MOMENTUM BACKFOLDING

The continuum model is expressed using the momenta of the monolayer, here denoted in capital letters $\mathbf{K}_\ell, \mathbf{K}'_\ell$ with layer index ℓ. The moiré potential folds the momenta back to a small mini-Brillouin zone (BZ) whose high-symmetry points are $\boldsymbol{\gamma} = (0, 0)$, $\boldsymbol{\kappa} = (\frac{4\pi}{3a_M}, 0)$, $\boldsymbol{\kappa}' = (\frac{2\pi}{3a_M}, \frac{2\pi}{\sqrt{3}a_M})$, and $\boldsymbol{\mu} = \frac{1}{2}\mathbf{g}_1$. The question is which monolayer momenta correspond to which mini-BZ momenta.

In Ref. [4], the authors map the monolayer **K** to the $\boldsymbol{\gamma}$ point of the mini-BZ. Such backfolding only occurs when the moiré length a_M is a multiple of three times the monolayer lattice constant [see Fig. 1(c)]. In general, however, this is not true: The moiré length in aligned commensurate cases can be expressed as $a_M = pa_1 = qa_2$ for coprime integers p, q. When both p, q are *not* multiples of three, the **K** points of the single layers map onto the $\boldsymbol{\kappa}$ points of the mini-BZ. This is the case for aligned WS_2/WSe_2 with $a_M = 25a_{WSe_2} = 26a_{WS_2}$ [22] and aligned $MoTe_2/WSe_2$ with $a_M = 13a_{MoTe_2} = 14a_{WSe_2}$ [29]. Therefore the relevant momentum backfolding to describe the experiments is $\mathbf{K}_1, \mathbf{K}'_2 \to \boldsymbol{\kappa}$ and $\mathbf{K}_2, \mathbf{K}'_1 \to \boldsymbol{\kappa}'$, as is shown in Fig. 1(a). For general incommensurate and possibly twisted moiré patterns we retain this mapping of momenta as shown in Fig. 1(b). Note that in the continuum theory of TMD homobilayers, the same mapping of momenta is used [12].

With the correct momentum backfolding, the valence band structure of aligned AA-stacked WS_2/WSe_2 and AB-stacked $MoTe_2/WSe_2$ are shown in Fig. 2. For WS_2/WSe_2, I use $a_M = 7.98$ nm, $m^* = 0.36m_e$, and the moiré potential $(V, \psi) = (7.7\text{ meV}, -106^\circ)$ is calculated using density functional theory with QUANTUM ESPRESSO [34,35] with a Coulomb cutoff [36] and the method of Ref. [4]. For $MoTe_2/WSe_2$, I use the parameters $a_M = 4.55$ nm, $m^* = 0.65m_e$, and $(V, \psi) = (7\text{ meV}, -14^\circ)$ based on Ref. [31]. The resulting flat bands have a very clear spin-orbit splitting at $\boldsymbol{\kappa}$ and $\boldsymbol{\kappa}'$. The general structure of spin/valley-split bands except along the line γ-μ was also observed in large-scale density functional theory (DFT) calculations of WS_2/WSe_2 [22] and $MoTe_2/WSe_2$ [29]. While the band structures are the same, none of these references actually derive a tight-binding model that can be used for strong-coupling studies. How to derive the tight-binding model will be discussed in the next section.

Note that in Fig. 2 the zero of energy corresponds to the valence band maximum in the monolayer. The Fermi level is tunable by electrostatic gating, and is therefore not shown.

IV. SYMMETRY ANALYSIS

The tight-binding model for the valence flat bands can be derived using symmetry arguments. Using these symmetry arguments, we can derive from specific continuum models [29,31] the correct values of spin-orbit coupling in the effective tight-binding model.

Let me first focus only on nearest-neighbor hopping t_1, since it is much larger than the longer-ranged hoppings t_2, t_3. The C_3 symmetry of the heterobilayer implies that t_1 can be complex, $t_1 = |t_1|e^{i\phi_1}$, as shown in Fig. 3(a). Within the continuum model of Eq. (1), the band structure has an *additional symmetry*: It is *sixfold* symmetric around the maximum of the flat band. For the band that has a maximum at $\boldsymbol{\kappa}$, its energy must be the same at $\boldsymbol{\kappa}'$ and $\boldsymbol{\gamma}$. For the nearest-neighbor hopping term, the energy at $\boldsymbol{\gamma}$ is $\epsilon_{\boldsymbol{\gamma}} = 6|t_1|\cos\phi_1$, whereas the energy at $\boldsymbol{\kappa}'$ is $\epsilon_{\boldsymbol{\kappa}'} = -3|t_1|(\cos\phi_1 + \sqrt{3}\sin\phi_1)$. Provided that the maximum of the band structure lies at $\boldsymbol{\kappa}$, equating $\epsilon_{\boldsymbol{\kappa}'} = \epsilon_{\boldsymbol{\gamma}}$ implies

$$\phi_1 = \frac{2\pi}{3}. \tag{2}$$

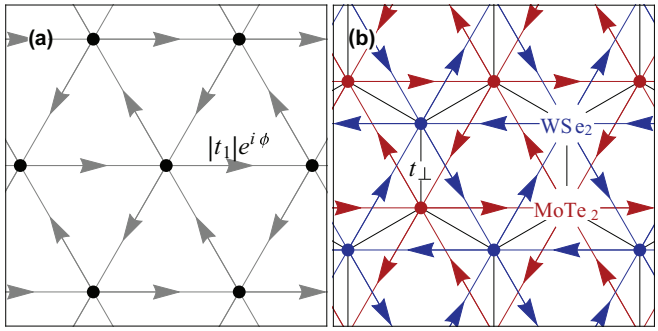

FIG. 3. (a) The effective model of a plain heterobilayer contains orbitals at triangular lattice sites with nearest-neighbor hopping $t_1 = |t_1|e^{i\phi}$ where the phase is spin dependent, $\phi = \frac{2\pi}{3}\sigma^z$. The states live completely within one monolayer. In the case of $MoTe_2/WSe_2$, the states are centered at the MM' sites in the $MoTe_2$ layer. (b) By tuning the vertical displacement field the second layer becomes relevant. The second layer, in the case of AB-stacked $MoTe_2/WSe_2$, is described by the same triangular lattice model with opposite spin-orbit coupling phases and a different moiré unit cell center XX'. As a result, the combination of in-plane spin-orbit coupling Eq. (5) and interlayer hopping Eq. (6) leads to an ideal realization of the Kane-Mele model.

Looking at nearest-neighbor hopping only, the sixfold symmetry of the continuum model therefore completely constrains the phase of the spin-orbit coupling. The resulting tight-binding model is thus a triangular lattice with spin-orbit coupled hopping,

$$H = t_1 \sum_{\langle ij\rangle\sigma} e^{i\phi\sigma^z \nu_{\langle ij\rangle}} c^\dagger_{i\sigma} c_{j\sigma}, \tag{3}$$

where $\nu_{\langle ij\rangle} = \pm 1$ depending on the direction of the bond, $\sigma^z = \pm 1$ indicates the z component of the electron spin, and $\phi = \frac{2\pi}{3}$. What is left is to derive the magnitude of the hopping $|t_1|$, and the positioning of the triangular lattice sites, both of which depend on the specific choice of heterobilayer compounds.

Because a honeycomb lattice is equivalent to two intertwined triangular lattices, we see that Eq. (3) corresponds for a single spin to the hopping model introduced by Haldane [37] for the Chern insulator. Including both spins, one finds that the Kane-Mele model of topological insulators [38,39], restricted to one honeycomb sublattice, is equal to Eq. (3) with $\phi = \pi/2$.

Note that the symmetry argument does *not* constrain the phase of the second-nearest-neighbor hopping $|t_2|e^{i\phi_2}$ on the triangular lattice. However, the *third*-nearest-neighbor hopping $t_3 = |t_3|e^{i\phi_3}$ is constrained, using the same expansion as above for ϕ_1, to have $\phi_3 = \frac{\pi}{3}$.

To verify the symmetry argument, I performed a Wannierization [40] of the flat bands derived in Fig. 2. For WS_2/WSe_2 this leads to

$$\begin{aligned} |t_1| &= 1.81 \text{ meV}, \quad \phi_1 = \frac{2\pi}{3}, \\ |t_2| &= 0.28 \text{ meV}, \quad \phi_2 = \pi, \\ |t_3| &= 0.11 \text{ meV}, \quad \phi_3 = \frac{\pi}{3}, \end{aligned} \tag{4}$$

consistent with the symmetry analysis. The spin-orbit coupling phases are the same for $MoTe_2/WSe_2$, but with $|t_1| = 4.03$ meV, $|t_2| = 0.92$ meV, and $|t_3| = 0.34$ meV.

V. TOPOLOGICAL TRANSITION IN $MoTe_2/WSe_2$

It has been argued that the observed topological transition in $MoTe_2/WSe_2$ [11] is due to a coupling to the states in the second layer [29,31], induced by a perpendicular electric field. There is, however, not yet a simple tight-binding model explaining this topological transition. Building on the model of Eq. (3), we can show how topologically nontrivial bands arise in a hopping model.

In the absence of an electric field, the valence flat band of $MoTe_2/WSe_2$ is localized in the MM' region of the $MoTe_2$ layer. In the other layer, the moiré potential localizes the top of the valence band at the XX' region. Furthermore, because the valence band top in the **K** valley of WSe_2 maps onto $\boldsymbol{\kappa}'$, we find that the effective tight-binding model for the WSe_2 states has an *opposite* phase $\phi = \mp\frac{2\pi}{3}$. The resulting two flat bands can therefore be represented by a honeycomb lattice as is shown in Fig. 3(b). The *intralayer* hopping in the $MoTe_2/WSe_2$ bilayer is represented by the spin-orbit coupling term

$$H = \sum_{\langle\langle ij\rangle\rangle\ell\sigma} t_\ell e^{i\ell\sigma^z \nu_{\langle\langle ij\rangle\rangle}\phi} c^\dagger_{i\ell\sigma} c_{j\ell\sigma}, \tag{5}$$

where $\langle\langle ij\rangle\rangle$ represents the next-nearest neighbor on the honeycomb lattice where $\nu_{\langle\langle ij\rangle\rangle} = \pm 1$ depends on the direction, $\ell = \pm 1$ the layer index, and $\sigma^z = \pm 1$ the spin. This is exactly the Kane-Mele spin-orbit coupling term [38,39].

The interlayer hopping is now given by *nearest-neighbor* hopping on the honeycomb lattice. The C_3 symmetry once again constrains the possible complex phases of the interlayer hopping, as described in Ref. [29]. For the tight-binding model this yields

$$H_\perp = t_\perp \sum_{\langle ij\rangle\sigma} e^{i\frac{2\pi}{3}\nu_{\langle ij\rangle}} c^\dagger_{i\ell\sigma} c_{j\bar{\ell}\sigma}, \tag{6}$$

where $\langle ij\rangle$ now couples the nearest neighbors on the honeycomb lattice. The parameter $\nu_{\langle ij\rangle} = 0$, 1, or 2 depends on the direction and increases counterclockwise when going around the $MoTe_2$ lattice sites. Equations (5) and (6) form an effective tight-binding model constrained by symmetry which is visualized in Fig. 3(b).

In the absence of an electric field the flat bands from the WSe_2 layer are at a much lower energy than the $MoTe_2$ states. A perpendicular electric field V can shift the WSe_2 states upward,

$$H_V = (V + \Delta) \sum_i n_{i,\ell=2}, \tag{7}$$

where $\Delta < 0$ is the band offset. By increasing V the bands from the two layers will overlap, at which point the interlayer coupling Eq. (6) becomes relevant. With $t_2 = 3.4$ meV extracted from the effective mass of the WSe_2 valence band and $t_\perp = 4$ meV, we calculate the band structure as a function of perpendicular field in Fig. 4. Above the critical field value V_c, a band inversion happens at the $\boldsymbol{\kappa}'$ point for the states in the **K** valley. For $V > V_c$, the top valence flat bands obtain a nonzero

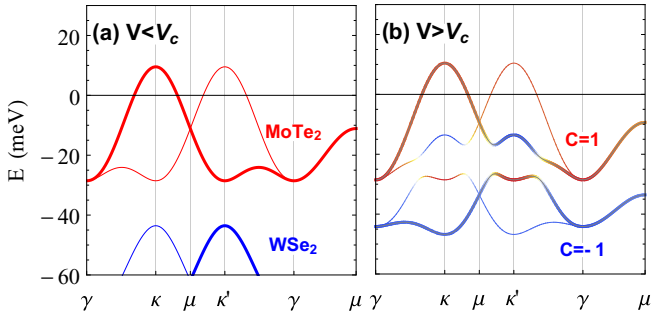

FIG. 4. (a) The flat valence bands in the $MoTe_2/WSe_2$ heterobilayer for the **K** valley (the opposite valley is shown in thin lines). The top flat band contains exclusively states in the $MoTe_2$ layer, whereas the bottom band contains exclusively states in the WSe_2 layer. (b) By tuning the perpendicular electric field V through a critical value, a band inversion occurs around the $\boldsymbol{\kappa}'$ point. The color scale indicates whether states live in the $MoTe_2$ layer (red) or WSe_2 layer (blue). The resulting bands carry a nonzero Chern number with opposite Chern numbers for opposite spin. This transition to a topological insulator band structure is described by the Kane-Mele model of Eqs. (5)–(7).

Chern number which is opposite for the two spin species [41]. As such, the system has become a topological insulator fully described by the honeycomb lattice model of Kane-Mele.

The effective Kane-Mele model applies to all TMD heterobilayers provided the applied perpendicular electric field is sufficient to overcome the valence band offset. The critical value V_c therefore depends on the bare band alignment Δ in the absence of a displacement field. For $MoTe_2/WSe_2$, shown in Fig. 4, we estimate the critical value to be $V_c = \Delta - 32.5$ meV.

VI. INTERACTIONS

The presence of spin-orbit coupling has some implications for the possible interacting states. In particular, at half filling of the topmost flat band in the limit of strong coupling, the complex hopping phases lead to an effective spin model with Dzyaloshinskii-Moriya (DM) interactions [27]. However, it was recently shown that the specific phase $\phi = \frac{2\pi}{3}$ for nearest-neighbor hopping can be gauged away [42], leaving only a nearest-neighbor Heisenberg term. As a result, the specific value of the spin-orbit coupling that I derived in this paper stabilizes an in-plane 120° antiferromagnetic order.

Inclusion of the displacement field, however, changes this picture. Chern bands at half filling are known to be susceptible to full spin polarization leading to a quantum anomalous Hall (QAH) effect [43,44]. The Mott-to-QAH transition observed in Ref. [11] can possibly be understood as a metamagnetic transition from in-plane Néel to Ising ferromagnetic order. A recent paper studied such a transition in a related Kane-Mele-like model with Hubbard interactions [30].

Note that within the current model, there is no band gap between the topologically nontrivial bands. However, interaction-driven renormalization of the bands can open up the gap at full filling of the top valence flat bands [31].

VII. CONCLUSION

I showed that by correctly mapping the monolayer momenta onto the mini-BZ, the effective model of TMD heterobilayers obtains a strong spin-orbit coupling as given by Eq. (3). The interlayer coupling can be described by a Kane-Mele model following Eqs. (5)–(7), yielding a topological transition as a function of perpendicular electric field.

Having an effective tight-binding model is an important step towards a full understanding of possible strongly correlated phases. This paper shows that spin-orbit coupling cannot be ignored in further studies of TMD heterobilayers.

ACKNOWLEDGMENTS

I thank Johannes Motruk, Kin Fai Mak, Fengcheng Wu, Allan MacDonald, Trithep Devakul, Vladimir Dobrosavljević, and Liang Fu for useful discussions. I acknowledge support by Swiss National Science Foundation via an Ambizione Grant No. PZ00P2_174208.

APPENDIX: MOIRÉ LENGTH

In this Appendix I will derive the expression for the moiré length a_M in terms of the lattice constants of the two layers $a_{1,2}$ and the twist angle θ. Without loss of generality, let us twist layer one with angle $+\theta/2$ and layer two with angle $-\theta/2$, so that the $\mathbf{K}_{1,2}$ points are at

$$\mathbf{K}_{1,2} = \frac{4\pi}{3a_{1,2}}(\cos\theta/2, \pm\sin\theta/2). \tag{A1}$$

Strictly speaking, the moiré length is only defined for commensurate twist angles and lattice mismatches. For general twist angle and lattice mismatch, following the Brillouin zone backfolding of Fig. 1(b), I use the fact that the corners of the mini-Brillouin zone (BZ) are given by $\mathbf{K}_1 = \boldsymbol{\kappa}$ and $\mathbf{K}_2 = \boldsymbol{\kappa}'$. In the mini-BZ, the distance between $\boldsymbol{\kappa}$ and $\boldsymbol{\kappa}'$ is equal to $\frac{4\pi}{3a_M}$. Consequently,

$$\frac{4\pi}{3a_M} = |\mathbf{K}_1 - \mathbf{K}_2| = \frac{4\pi}{3}\sqrt{\frac{1}{a_1^2} + \frac{1}{a_2^2} - \frac{2\cos\theta}{a_1 a_2}}. \tag{A2}$$

[1] E. Y. Andrei and A. H. MacDonald, Graphene bilayers with a twist, Nat. Mater. **19**, 1265 (2020).
[2] S. Carr, S. Fang, and E. Kaxiras, Electronic-structure methods for twisted moiré layers, Nat. Rev. Mater. **5**, 748 (2020).
[3] L. Balents, C. R. Dean, D. K. Efetov, and A. F. Young, Superconductivity and strong correlations in moiré flat bands, Nat. Phys. **16**, 725 (2020).
[4] F. Wu, T. Lovorn, E. Tutuc, and A. H. MacDonald, Hubbard Model Physics in Transition Metal Dichalcogenide Moiré Bands, Phys. Rev. Lett. **121**, 026402 (2018).
[5] Y. Tang, L. Li, T. Li, Y. Xu, S. Liu, K. Barmak, K. Watanabe, T. Taniguchi, A. H. MacDonald, J. Shan, and K. F. Mak, Simulation of Hubbard model physics in WSe_2/WS_2 moiré superlattices, Nature (London) **579**, 353 (2020).

[6] T. Li, S. Jiang, L. Li, Y. Zhang, K. Kang, J. Zhu, K. Watanabe, T. Taniguchi, D. Chowdhury, L. Fu, J. Shan, and K. F. Mak, Continuous Mott transition in semiconductor moiré superlattices, Nature (London) **597**, 350 (2021).

[7] E. C. Regan, D. Wang, C. Jin, M. I. Bakti Utama, B. Gao, X. Wei, S. Zhao, W. Zhao, Z. Zhang, K. Yumigeta, M. Blei, J. D. Carlström, K. Watanabe, T. Taniguchi, S. Tongay, M. Crommie, A. Zettl, and F. Wang, Mott and generalized Wigner crystal states in WSe_2/WS_2 moiré superlattices, Nature (London) **579**, 359 (2020).

[8] Y. Xu, S. Liu, D. A. Rhodes, K. Watanabe, T. Taniguchi, J. Hone, V. Elser, K. F. Mak, and J. Shan, Correlated insulating states at fractional fillings of moiré superlattices, Nature (London) **587**, 214 (2020).

[9] X. Huang, T. Wang, S. Miao, C. Wang, Z. Li, Z. Lian, T. Taniguchi, K. Watanabe, S. Okamoto, D. Xiao, S.-F. Shi, and Y.-T. Cui, Correlated insulating states at fractional fillings of the WS_2/WSe_2 moiré lattice, Nat. Phys. **17**, 715 (2021).

[10] C. Jin, Z. Tao, T. Li, Y. Xu, Y. Tang, J. Zhu, S. Liu, K. Watanabe, T. Taniguchi, J. C. Hone, L. Fu, J. Shan, and K. F. Mak, Stripe phases in WSe_2/WS_2 moiré superlattices, Nat. Mater. **20**, 940 (2021).

[11] T. Li, S. Jiang, B. Shen, Y. Zhang, L. Li, Z. Tao, T. Devakul, K. Watanabe, T. Taniguchi, L. Fu, J. Shan, and K. F. Mak, Quantum anomalous Hall effect from intertwined moiré bands, Nature (London) **600**, 641 (2021).

[12] F. Wu, T. Lovorn, E. Tutuc, I. Martin, and A. H. MacDonald, Topological Insulators in Twisted Transition Metal Dichalcogenide Homobilayers, Phys. Rev. Lett. **122**, 086402 (2019).

[13] L. J. McGilly, A. Kerelsky, N. R. Finney, K. Shapovalov, E.-M. Shih, A. Ghiotto, Y. Zeng, S. L. Moore, W. Wu, Y. Bai, K. Watanabe, T. Taniguchi, M. Stengel, L. Zhou, J. Hone, X. Zhu, D. N. Basov, C. Dean, C. E. Dreyer, and A. N. Pasupathy, Visualization of moiré superlattices, Nat. Nanotechnol. **15**, 580 (2020).

[14] A. Weston, Y. Zou, V. Enaldiev, A. Summerfield, N. Clark, V. Zólyomi, A. Graham, C. Yelgel, S. Magorrian, M. Zhou, J. Zultak, D. Hopkinson, A. Barinov, T. H. Bointon, A. Kretinin, N. R. Wilson, P. H. Beton, V. I. Fal'ko, S. J. Haigh, and R. Gorbachev, Atomic reconstruction in twisted bilayers of transition metal dichalcogenides, Nat. Nanotechnol. **15**, 592 (2020).

[15] Z. Zhang, Y. Wang, K. Watanabe, T. Taniguchi, K. Ueno, E. Tutuc, and B. J. LeRoy, Flat bands in twisted bilayer transition metal dichalcogenides, Nat. Phys. **16**, 1093 (2020).

[16] S. Shabani, S. Liu, J. Hone, X. Zhu, and A. N. Pasupathy, Deep moiré potentials in twisted transition metal dichalcogenide bilayers, Nat. Phys. **17**, 720 (2021).

[17] Y. Zhang, N. F. Q. Yuan, and L. Fu, Moiré quantum chemistry: Charge transfer in transition metal dichalcogenide superlattices, Phys. Rev. B **102**, 201115(R) (2020).

[18] Y. Zhang, T. Liu, and L. Fu, Electronic structures, charge transfer, and charge order in twisted transition metal dichalcogenide bilayers, Phys. Rev. B **103**, 155142 (2021).

[19] B. Padhi, R. Chitra, and P. W. Phillips, Generalized Wigner crystallization in moiré materials, Phys. Rev. B **103**, 125146 (2021).

[20] V. Vitale, K. Atalar, A. A. Mostofi, and J. Lischner, Flat band properties of twisted transition metal dichalcogenide homo- and heterobilayers of MoS_2, $MoSe_2$, WS_2 and WSe_2, 2D Mater. **8**, 045010 (2021).

[21] H. Li, S. Li, M. H. Naik, J. Xie, X. Li, E. Regan, D. Wang, W. Zhao, K. Yumigeta, M. Blei, T. Taniguchi, K. Watanabe, S. Tongay, A. Zettl, S. G. Louie, M. F. Crommie, and F. Wang, Imaging local discharge cascades for correlated electrons in WS_2/WSe_2 moiré superlattices, Nat. Phys. **17**, 1114 (2021).

[22] H. Li, S. Li, M. H. Naik, J. Xie, X. Li, J. Wang, E. Regan, D. Wang, W. Zhao, S. Zhao, S. Kahn, K. Yumigeta, M. Blei, T. Taniguchi, K. Watanabe, S. Tongay, A. Zettl, S. G. Louie, F. Wang, and M. F. Crommie, Imaging moiré flat bands in three-dimensional reconstructed WSe_2/WS_2 superlattices, Nat. Mater. **20**, 945 (2021).

[23] M. H. Naik, S. Kundu, I. Maity, and M. Jain, Origin and evolution of ultraflat bands in twisted bilayer transition metal dichalcogenides: Realization of triangular quantum dots, Phys. Rev. B **102**, 075413 (2020).

[24] M. H. Naik and M. Jain, Ultraflatbands and Shear Solitons in Moiré Patterns of Twisted Bilayer Transition Metal Dichalcogenides, Phys. Rev. Lett. **121**, 266401 (2018).

[25] H. Pan and S. Das Sarma, Interaction-Driven Filling-Induced Metal-Insulator Transitions in 2D Moiré Lattices, Phys. Rev. Lett. **127**, 096802 (2021).

[26] H. Pan, F. Wu, and S. Das Sarma, Quantum phase diagram of a Moiré-Hubbard model, Phys. Rev. B **102**, 201104(R) (2020).

[27] H. Pan, F. Wu, and S. Das Sarma, Band topology, Hubbard model, Heisenberg model, and Dzyaloshinskii-Moriya interaction in twisted bilayer WSe_2, Phys. Rev. Research **2**, 033087 (2020).

[28] Y.-M. Xie, C.-P. Zhang, J.-X. Hu, K. F. Mak, and K. T. Law, Valley-Polarized Quantum Anomalous Hall State in Moiré $MoTe_2/WSe_2$ Heterobilayers, Phys. Rev. Lett. **128**, 026402 (2022).

[29] Y. Zhang, T. Devakul, and L. Fu, Spin-textured Chern bands in AB-stacked transition metal dichalcogenide bilayers, Proc. Natl. Acad. Sci. USA **118**, e2112673118 (2021).

[30] T. Devakul and L. Fu, Quantum anomalous Hall effect from inverted charge transfer gap, arXiv:2109.13909.

[31] H. Pan, M. Xie, F. Wu, and S. Das Sarma, Topological Phases in AB-stacked $MoTe_2/WSe_2$: $\mathbb{Z}_2$ Topological Insulators, Chern Insulators, and Topological Charge Density Waves, arXiv:2111.01152.

[32] F. Wu, T. Lovorn, and A. H. MacDonald, Theory of optical absorption by interlayer excitons in transition metal dichalcogenide heterobilayers, Phys. Rev. B **97**, 035306 (2018).

[33] F. Wu, T. Lovorn, and A. H. MacDonald, Topological Exciton Bands in Moiré Heterojunctions, Phys. Rev. Lett. **118**, 147401 (2017).

[34] P. Giannozzi, O. Andreussi, T. Brumme, O. Bunau, M. Buongiorno Nardelli, M. Calandra, R. Car, C. Cavazzoni, D. Ceresoli, M. Cococcioni, N. Colonna, I. Carnimeo, A. Dal Corso, S. de Gironcoli, P. Delugas, R. A. J. DiStasio, A. Ferretti, A. Floris, G. Fratesi, G. Fugallo *et al.*, Advanced capabilities for materials modelling with Quantum ESPRESSO, J. Phys.: Condens. Matter **29**, 465901 (2017).

[35] P. Giannozzi, S. Baroni, N. Bonini, M. Calandra, R. Car, C. Cavazzoni, D. Ceresoli, G. L. Chiarotti, M. Cococcioni, I. Dabo, A. Dal Corso, S. de Gironcoli, S. Fabris, G. Fratesi, R. Gebauer, U. Gerstmann, C. Gougoussis, A. Kokalj, M. Lazzeri, L. Martin-Samos *et al.*, QUANTUM ESPRESSO: A modular and open-source software project for quantum simulations of materials, J. Phys.: Condens. Matter **21**, 395502 (2009).

[36] T. Sohier, M. Calandra, and F. Mauri, Density functional perturbation theory for gated two-dimensional heterostructures: Theoretical developments and application to flexural phonons in graphene, Phys. Rev. B **96**, 075448 (2017).

[37] F. D. M. Haldane, Model for a Quantum Hall Effect without Landau Levels: Condensed-Matter Realization of the "Parity Anomaly", Phys. Rev. Lett. **61**, 2015 (1988).

[38] C. L. Kane and E. J. Mele, Quantum Spin Hall Effect in Graphene, Phys. Rev. Lett. **95**, 226801 (2005).

[39] C. L. Kane and E. J. Mele, Z_2 Topological Order and the Quantum Spin Hall Effect, Phys. Rev. Lett. **95**, 146802 (2005).

[40] N. Marzari, A. A. Mostofi, J. R. Yates, I. Souza, and D. Vanderbilt, Maximally localized Wannier functions: Theory and applications, Rev. Mod. Phys. **84**, 1419 (2012).

[41] T. Fukui, Y. Hatsugai, and H. Suzuki, Chern numbers in discretized Brillouin zone: Efficient method of computing (spin) Hall conductances, J. Phys. Soc. Jpn. **74**, 1674 (2005).

[42] D. Kiese, Y. He, C. Hickey, A. Rubio, and D. M. Kennes, TMDs as a platform for spin liquid physics: A strong coupling study of twisted bilayer WSe_2, APL Materials **10**, 031113 (2022).

[43] N. Bultinck, S. Chatterjee, and M. P. Zaletel, Mechanism for Anomalous Hall Ferromagnetism in Twisted Bilayer Graphene, Phys. Rev. Lett. **124**, 166601 (2020).

[44] L. Rademaker, I. V. Protopopov, and D. A. Abanin, Topological flat bands and correlated states in twisted monolayer-bilayer graphene, Phys. Rev. Research **2**, 033150 (2020).